scientific reports

Check for updates

OPEN

Visualization of non-Newtonian convective fluid flow with internal heat transfer across a rotating stretchable surface impact of chemical reaction

Zeeshan[1]✉, Ilyas Khan[2], Nosheen Feroz[1], Fuad S. Al-Duais[3,4] & Omar Mahmoud[5]

The present investigation focuses on the characteristics of heat and mass transfer in the context of their applications. There has been a lot of interest in the use of non-Newtonian fluids in engineering and biological disciplines. Having such considerable attention to non-Newtonian fluids, the goal is to explore the flow of Jeffrey non-Newtonian convective fluid driven by a non-linear stretching surface considering the effect of nonlinear chemical reaction effect. The relevant set of difference equations was changed to ordinary equations by using a transformation matrix. To create numerical solutions for velocity and concentration fields, the Runge–Kutta fourth-order method along with the shooting approach is utilized. The innovative fragment of the present study is to scrutinize the magnetized viscous non-Newtonian fluid over extending sheet with internal heat transfer regarding the inspiration of nonlinear chemical reaction effect, which still not has been elaborated on in the available works to date. Consequently, in the restrictive sense, the existing work is associated with available work and originated in exceptional agreement. Graphs depict the effects of various variables on motion and concentration fields, like the Hartman number, Schmidt number, and chemical reaction parameter. The performance of chemical reaction factor, Schmidt number, Hartmann number, and Deborah numbers on velocities component, temperature, and concentration profiles are discussed through graphs. The effect of emerging parameters in the mass transfer is also investigated numerically and 3D configuration is also provided. It is observed that the Deborah numbers and Hartmann numbers have the same effect on velocity components. Also, the thickness of the boundary layer reduces as the Hartmann number increases. As the Schmit number grows, the concentration field decline. For destructive and generative chemical reactions, the concentration fields observed opposite effects. It is also noticed that the surface mas transfer reduces as the Hartmann number rises. The statistical findings of the heat-transfer rate are also documented and scrutinized.

Non-Newtonian materials have received a lot of attraction in recent decades due to technical and materials science. Non-Newtonian activity can be observed in coating sheets, foodstuffs, fiber optics, digging muds, and thermoplastic polymers production processes. The Jeffrey liquid is one of the fluid models that have received a lot of interest from researchers. Relaxing and delay reactions may occur with this flow model. Extrusion operations, crystal and sheet manufacturing, semiconductor circuits, crystal growth, and other fields all benefit from studying boundary layer movements over a stretching cylinder. The boundary layer movement was introduced by Sakiadis[1] beyond a continuous solid substrate flowing at a consistent rate. Many researchers expanded on Sakiadis' theory for stretching sheet moments in viscoelastic and non-Newtonian liquids heat fluxes under variable circumstances. The articles[2–10] reflect some of the most recent work on the subject. Flows induced by a vertical

[1]Department of Mathematics and Statistics, Bacha University Charsadda, Charsadda, KP 24420, Pakistan. [2]Department of Mathematics, College of Science, Al-Zulfi, Majmaah University, Majmaah 11952, Saudi Arabia. [3]Department of Mathematics, College of Science and Humanities in Al-Aflaj, Prince Sattam bin Abdulaziz University, Al-Kharj, Al-Aflaj 11942, Saudi Arabia. [4]Administration Department, Administrative Science College, Thamar University, Thamar, Yemen. [5]Petroleum Engineering Department, Faculty of Engineering and Technology, Future University in Egypt, New Cairo 11835, Egypt. ✉email: zeeshan@bkuc.edu.pk

stretched surface are considered in almost all of the research listed above. Some studies[11–15] may also be addressed in these aspects. Raptis and Perdikis[16] focused at magnetized viscous flow across a stochastic extending surface in the occurrence of a chemical process recently. The goal of this research is to (1) expand flow characteristics to Jeffrey liquids[16] and (2) propose an numerical solution for a nonlinear dynamic situation.

For the numerical solution, a newly developed methodology called the Killer-box-method[17] was used. Similar issues have been effectively solved using this strategy[18,19,19,19–30].

The transport of convective heat can be improved by modifying the flow shape, the operating conditions, or by increasing the thermal sensitivity. For example, adding tiny particles with high electrical stability to a fluid improves its overall thermal properties. The microscopic droplets are referred to as nanostructures, and the solvent with no additives is referred to as conventional fluids, which includes water, methane, kerosene, and so on. There are two methods for depositing these nanoparticles; the first one is known as the single-step approach[31] via direct vaporization. The second process, known as the two-step technique generated nanoparticles individually and subsequently disseminated them in the conventional fluids. Many studies have been conducted to study the characteristics that influence the nanoparticle's resistance to heat flux. Unlike microbes, nanomaterial's are not conscience; their movement is driven by Brownian motion and thermophoresis. The thicker microbes sink into the coolant, and indeed the microbes float to the surface. This replenishment causes a macroscopic movement known as bioconvection. Many studies[32] purported to show the emergence of motile bacteria in nanofluid momentum. The heat transmission problem was examined employing Fourier law, but proved being too difficult to observe. Subsequently, with the assistance of Cattaneo and, later Christov[33–37], a refined Fourier law was devised and applied to define and evaluate the heat transmission problem beyond extending cylinders.

Turkyilmazoglu[38] investigated the longitudinal fins of rectangular profile past a stretching sheet and examined the heat transfer phenomena. The heat-mass transfer of magnetofydrodynamic flow over a permeable rotating sheet with variable viscosity was examined by Turkyilmazoglu[39]. Turkyilmazoglu[40] studied the convection MHD flow with porous matrix and heat source. A closed form of solutions has been obtained for the thermal radiation. Similarly, Turkyilmazoglu[41] investigated the dust Nano sized particles past a stretchable rotating sheet with two-phase heat analysis. The nonlinear solution has been obtained and discussed the convergence of adomian decomposition method by Turkyilmazoglu[41]. The heat transfer analysis with variable Prandtl numbers over a rotating disk of MHD flow with uniform electric field was explored by Turkyilmazoglu[42]. The hybrid nanofluid fluid with thermal radiation over a porous stretchable sheet with partial slip was examined by Turkyilmazoglu et al.[43].

The innovative fragment of the present study is to scrutinize the magnetized viscous non-Newtonian fluid over extending sheet with internal heat transfer regarding the inspiration of variable viscosity and multiple slip effect, still not has been elaborated in the available works to date. Consequently, in the restrictive sense, the existing work is associated with available work and originated in exceptional agreement. It is observed that the Deborah numbers and Hartmann number have same effect on velocity components. Also the thickness of the boundary layer reduces as the Hartmann number increases. As the Schmidt number grows, the concentration field decline. For destructive and generative chemical reactions, the concentration fields observed opposite effects. It is also noticed that the surface mas transfer reduces as Hartmann number rising. The statistical findings of the heat-transfer rate are also documented and scrutinized.

The goal of the present study is to investigate the characteristics of heat and mass transfer in the context of their applications. There has been a lot of interest in the use of non-Newtonian fluids in engineering and biological disciplines. Having such a considerable attention in non-Newtonian fluids, the goal is to explore the flow of Jeffrey non-Newtonian mixed convective fluid driven by a non-linear permeable rotating stretching surface considering with suction or injection and nonlinear thermal radiation effect. The relevant set of difference equations was changed to ordinary equations by using a transformation matrix. To create numerical solutions for velocity and concentration fields, the Runge–Kutta fourth-order method along with the shooting approach is utilized.

The following is the outline of the presentation. The problem's concept is presented in " Mathematical modelling" section. "Numerical procedure and validation of code" section deduces velocity and concentration numerical solutions. The consolidation of the resulting solutions is explicitly examined in "Results and discussion" section. The explanation of graphical form is covered in "Closing remarks" section. Section 6 summarises the findings.

Mathematical modelling

Figure 1 shows the geometry of the problem. A 2D Jeffrey liquid that flows across a magnetized stretched surface is considered. It is assumed that the x-axis is along the stretch sheet, while the y-axis is vertical. In the y-direction, a homogeneous magnetic flux exerts its influence. The resultant magnetic force is ignored for tiny magnetic Reynolds numbers. We also took into account the possibility of a first-order reaction.

The equations that regulate the stream in this situation are as follows[9,12,14]:

$$\frac{\partial u}{\partial x}+\frac{\partial v}{\partial y}=0 \tag{1}$$

$$\begin{aligned} u\frac{\partial u}{\partial x}+v\frac{\partial u}{\partial y} &= \lambda_1\left(u^2\frac{\partial^2 u}{\partial x^2}+v^2\frac{\partial^2 u}{\partial y^2}+2uv\frac{\partial^2 u}{\partial y\partial x}\right)\\ &= \nu\left(\frac{\partial^2 u}{\partial y^2}+\lambda_2\left(u\frac{\partial^2 u}{\partial y^2\partial x}+v\frac{\partial^3 u}{\partial y^3}-\frac{\partial u}{\partial x}\frac{\partial^2 u}{\partial y^2}-\frac{\partial u}{\partial x}\frac{\partial^2 u}{\partial y^2}\right)\right)-\frac{\sigma B_0^2}{\rho} \end{aligned} \tag{2}$$

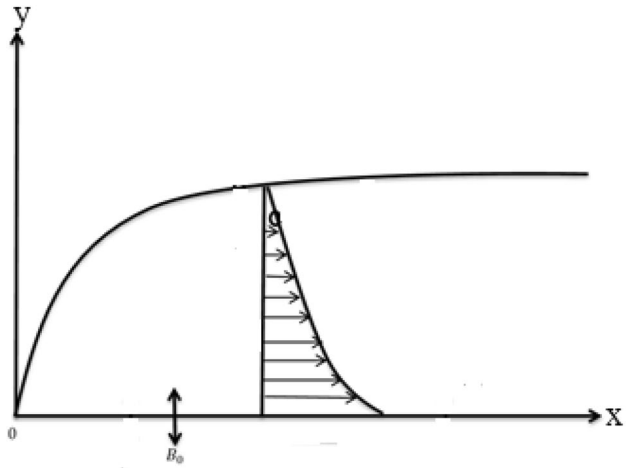

Figure 1. Geometry of the mathematical modelling.

$$u\frac{\partial T}{\partial x} + v\frac{\partial T}{\partial y} = D\frac{\partial^2 T}{\partial y^2} - RT \tag{3}$$

In the upstairs balances, u and v are velocities lengthwise x and y-directions, individually, ν the kinematic viscosity, ρ the density, σ the conductivity, λ_1, λ_2 the relaxation/retardation time, T the concentration, D the diffusion quantity, and R is the reaction factor.

The suitable constraints are[9,10]

$$\begin{aligned} &u(x,y) = a_1 x + b_1 x^2 \\ &v(x,y) = 0, T(x,y) = T_w \, at \, y = 0 \\ &u \to 0, T \to 0 \, as \, y \to \infty \end{aligned} \tag{4}$$

here a_1 and b_1 are assumed to be constants.

For simplicity of the problem, we familiarize the following similarities:

$$\begin{aligned} &\eta = \left(\frac{a_1}{\nu}\right)^{\frac{1}{2}} y, u = a_1 x f^{'}(\eta) + b_1 x^2 g^{'}(\eta), v = -(a_1 \nu)^{\frac{1}{2}} f(\eta) - 2b_1 x \left(\frac{\nu}{a_1}\right)^{\frac{1}{2}} g(\eta), \\ &T = T_w \left(T_0(\eta) + \frac{2b_1 x}{a_1} T_1(\eta)\right) \end{aligned} \tag{5}$$

here prime signifies the derivative with reverence to η. Equation 1 is pleased automatically and Eqs. (2–4) are distorted as monitors:

$$\begin{aligned} &f'''(\eta) + M^2 f'(\eta) - f'(\eta)^2 + f(\eta) f''(\eta) + \Omega_1 \left(2f(\eta) f'(\eta) f''(\eta) - f(\eta)^2 f''''(\eta)\right) \\ &+ \Omega_2 \left(f''(\eta)^2 - f(\eta) f''''(\eta)\right) = 0 \end{aligned} \tag{6}$$

$$\begin{aligned} &g'''(\eta) - M^2 g'(\eta) - 3f'(\eta) g'(\eta) + 2g(\eta) f''(\eta) + f'(\eta) g''(\eta) \\ &+ \Omega_1 \begin{pmatrix} 4f(\eta) f'(\eta) g''(\eta) + 2f(\eta) g'(\eta) f''(\eta) - f(\eta)^2 g'''(\eta) - 4f(\eta) g(\eta) f''''(\eta) \\ +4f'(\eta) g(\eta) f''(\eta) - 2f'(\eta)^2 g'(\eta) \end{pmatrix} \\ &+ \Omega_2 \left(f'(\eta) g''''(\eta) - g'(\eta) f''''(\eta) - f(\eta) g''''(\eta) - 2g(\eta) f''''(\eta) + 3f''(\eta) g''(\eta)\right) = 0 \end{aligned} \tag{7}$$

$$T_0'' + Scf T_0' - Sc\Upsilon T_0 = 0 \tag{8}$$

$$T_1'' + Scf(\eta) T_1' - Scf'(\eta) T_1 - Sc\Upsilon T_1 + Scg(\eta) T_0' = 0 \tag{9}$$

$$\begin{aligned} &f = 0, f' = 1, g = 0, g' = 1, T_0 = 1, T_1 = 0; \text{ at } \eta \to 0 \\ &f' = 0, g' = 0, T_0 = 0, T_1 = 0; \text{ at } \eta \to \infty \end{aligned} \tag{10}$$

In above equations Υ denotes chemical reaction factor, Sc stands for Schmidt number, M is the Hartman number, and Ω_1 ,Ω_2 are the Deborah numbers which are defiend as

Sc	Υ	M	$\Omega_1 = \Omega_2$	$-T_0'(0)$	$-T_1'(0)$	Liao[21] $-T_0'(0)$	Liao[21] $-T_1'(0)$
1	0.3	0.5	0.3	0.7230	0.1453	0.7231	0.1451
	0.7			0.8471	0.1414	0.8472	0.1412
	1.2			1.0447	0.1352	1.0443	0.1354
	1.8			1.3261	0.1140	1.3260	0.1146
0.4	2.2			0.9832	0.0291	0.9831	0.0299
0.8				0.9982	0.0954	0.9984	0.0951
1.2				1.3164	0.1543	1.3161	0.1546
1.6				1.5514	0.1950	1.5519	0.1952
2.2	1.3	0		1.2664	0.1347	1.2667	0.1347
		0.2		1.2542	0.1368	1.2543	0.1367
		0.4		1.1320	0.1377	1.1321	0.1376
		0.8		1.1142	0.1386	1.1142	0.1380
		1.0		1.0531	0.1399	1.0532	0.1393
		1.8	0	1.2537	0.1235	1.2536	0.1237
			0.3	1.2680	0.1343	1.2683	0.1348
			0.9	1.2884	0.1352	1.2887	0.1351
			1.2	1.2910	0.1367	1.2912	0.1360
			1.5	1.2997	0.1380	1.2991	0.1382

Table 1. Comparison of the variation of surface mass transfer $-T_0'(0)$ and $-T_1'(0)$ for some values of Sc, Υ, M $\Omega_1 = \Omega_2$ with published work[21].

$$\Upsilon = \frac{R}{a_1}, S = \frac{\nu}{D}, M_1^2 = \frac{\sigma B_0^2}{a_1 \rho}, \Omega_1 = \lambda_1 a_1, \Omega_2 = \lambda_2 a_1. \tag{11}$$

The expressions of the mass transfer T_0 and T_1 at the wall are

$$\begin{aligned} T_0'(0) &= \left(\frac{\partial T_0}{\partial \eta}\right)_{\eta=0} \leq 0, \\ T_1'(0) &= \left(\frac{\partial T_1}{\partial \eta}\right)_{\eta=0} \leq 0, \end{aligned} \tag{12}$$

Numerical procedure and validation of code

The scheme of Eqs. (6–10) are treated numerically by Runge–Kutta 4th order-scheme. For this goal the governing equivalences are transformed to the conventional differential balances by the resemblance conversion. The transformed set of equations is further altered into order-first differential equations. The relevant constraints are also transformed to the initial constraints. Applying the numerical method (RK4), the transformed dimensionless system of equations is calculated using step size $\Delta\eta = 0.01$. The current study is associated with published (see Table 1). The repetition practice is clogged up to meeting situations 10^{-5}. For endorsement of the consequences, the BVPh2 is also functional and admirable settlement is established as revealed in Fig. 2. The procedure of the numerical method is given in Fig. 3.

Results and discussion

In this work we have investigated the mixed convection flow of a Jeffrey non-Newtonian fluid over a stretchable surface. The problem is modelled and then solved numerically using the Runge–Kutta fourth-order method together with the shooting technique. The physical model of the problem is shown in Fig. 1. Numerical results are computed in terms of plots and table. Figures 2 and 3, are discussed in "Numerical procedure and validation of code" section. These plots depict the effects of various variables on motion and concentration fields, like the Hartman number, Schmidt number, and chemical reaction parameter. On f' and g', the performance of Ω_1 and M_1 is same. The thickness of the boundary layer is reduced when the value of M_1 is increased. As Sc grows, the concentration fields T_0 and T_1 decline. The destructive response ($\Upsilon > 0$) has the effect of lowering the concentration profiles. For destructive ($\Upsilon > 0$) and generative ($\Upsilon < 0$) chemical reactions, the concentration fields T_0 and T_1 observed opposite effects. By raising M_1, the surface mass transfer reduces. The statistical findings of the heat-transfer rate are also documented and scrutinized.

The pictorial results for the influence of Deborah numbers Ω_1, Ω_2 Hartman number M, Schmidt number Sc, and the chemical reaction factor Υ on f' and g' are shown in this section. Figures 4, 5, 6, 7, 8, 9, 10, 11, 12, 13, 14, 15, 16, 17, 18, 19, 20, 21, 22, 23, 24 and 25 provide examples of such impacts with physical amplifications.

The consequences of Ω_1, Ω_2 and M on f' and g' are examined in Figs. 4, 5, 6 and 7.

Figures 4 and 5 show the flow characteristics for varying parameter of Deborah number Ω_1 in the presence and absence of M. It is detected that, f' and g' decline across the boundary layer with the growing values of Ω_1.

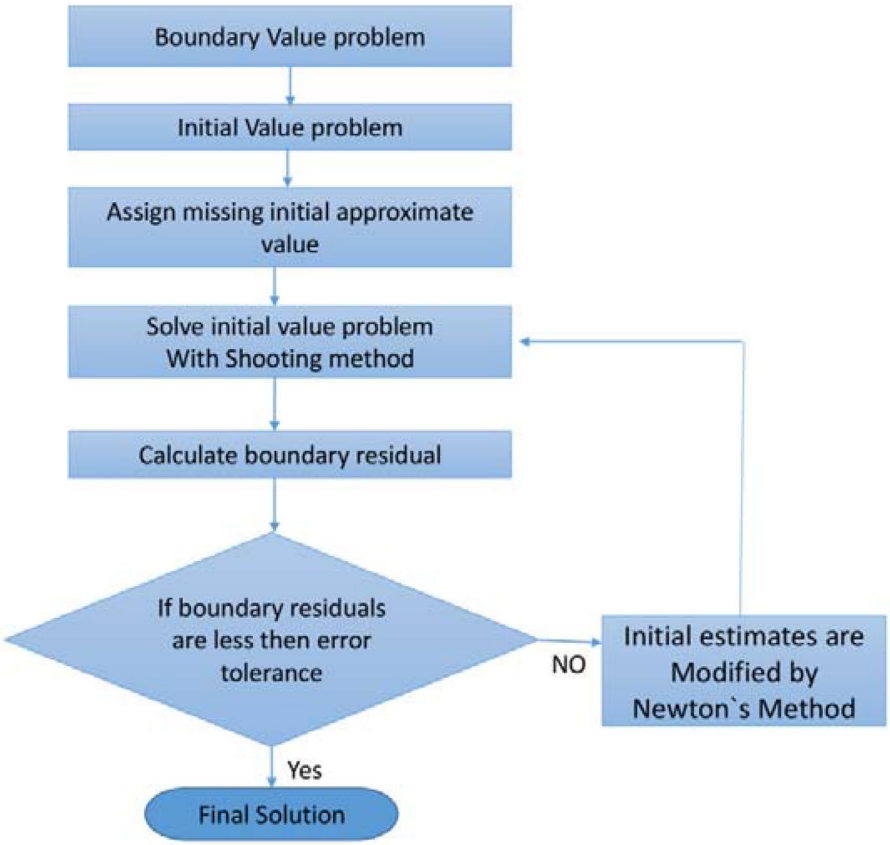

Figure 2. Flow chart of the numerical scheme.

The velocity profiles f' and g' are shown to be decreased as Ω_1 rises. When compared to g', however, the upsurge in f' is smaller. As Deborah number Ω_1 is enhanced, the film thickness reduces. In contrast the Deborah number Ω_2 has an opposite influence on the velocities f' and g' than Ω_1 as shown in Figs. 6 and 7.

From these figures it is clear crystal the influence of Ω_1 and Ω_2 on f' and g' is higher in the absence of M. Figures 8 and 9 display that the inspiration of the Hartman number M on the velocities f' and g' in the presence and absence of Deborah number. Figure 8 displays the influence of M on the velocity component f' which is a function of η . It is observed that the velocity reduces as the M raising. Also, from Fig. 9, it is quite evident that the velocity g' significantly decline as the M increases. The effect of M on f' and g' is analogous to that of Ω_1. From this analysis it is also investigated that the effect of M for $\Omega_2 = 0.4$ is higher than $\Omega_2 = 0.3$.

Figures 10, 11, 12, 13, 14, 15, 16, 17, 18, 19, 20 and 21 show the fluctuations of the entrepreneurs on the concentration components T_0 and T_1. Figures 10 and 11 demonstrate the impact of Deborah number Ω_1 on T_0 and T_1 in the event of a destructive chemical change ($\Upsilon > 0$). Whenever the value of Ω_1 is higher, the amplitude of the concentration profile T_0 grows, whereas the magnitude of T_1 drops. It should be noted that for high values of Ω_1, the variance in T_1 is greater than that in T_0.

In the event of a destructive chemical reaction ($\Upsilon > 0$), Figs. 12 and 13 explore the fluctuations of Ω_2 on the concentration fields T_0 and T_1 for two different values of M = 0 and M = 0.3. When linking Figs. 10 and 11, it can be seen that Figs. 12 and 13 have the opposite qualitative consequences. Also, for M = 0, the concentration fields rapidly decreases as compare with M = 0.3.

The consequence of Hartmann number M on T_0 and T_1 is seen in Figs. 14 and 15 respectively in the presence of Deborah numbers $\Omega_1 = 0.3$ and $\Omega_2 = 0.4$. As M is enhanced, the concentration fields T_0 and T_1 are found to increase. In both cases the enhancement is more significant for large value of Deborah number i.e., for $\Omega_2 = 0.4$.

Figures 16 and 17 show how the Schmidt number Sc varies upon concentration profiles T_0 and T_1. When Sc grows, respectively,T_0 and T_1 drop. Figures 18 and 19 depict the impact of the disruptive chemical reaction factor ($\Upsilon > 0$) on profiles T_0 and T_1. The concentration profile T_0 and T_1 are revealed to be a decreasing function of Υ. It's also evident that as Υ improves, the strength of T_0 and T_1 reduce.

Figures 20 and 21 reveal how the concentration profiles T_0 and T_1 change as a generating chemical reaction ($\Upsilon < 0$) progresses. On the other hand, when T_0 grows for large generating chemical reaction parameters, as seen in Fig. 18. The amplitude of T_1 grows as Υ ($\Upsilon < 0$) grows, as shown in Fig. 21.

The effect of Sc and Υ on mass transfer $T_0'(0)$ and $T_1'(0)$ is shown in Figs. 22 and 23. It is revealed that the superficial mass transfer T_0 enhances while T_1 reduces as Sc and Υ are increasing. Figures 24 and 25 show the influence of M and Sc on the $T_0'(0)$ and $T_1'(0)$. From these figures, it is clear form this figure that as M increases, the surface mass transfer T_0 decreases and T_1 enhances.

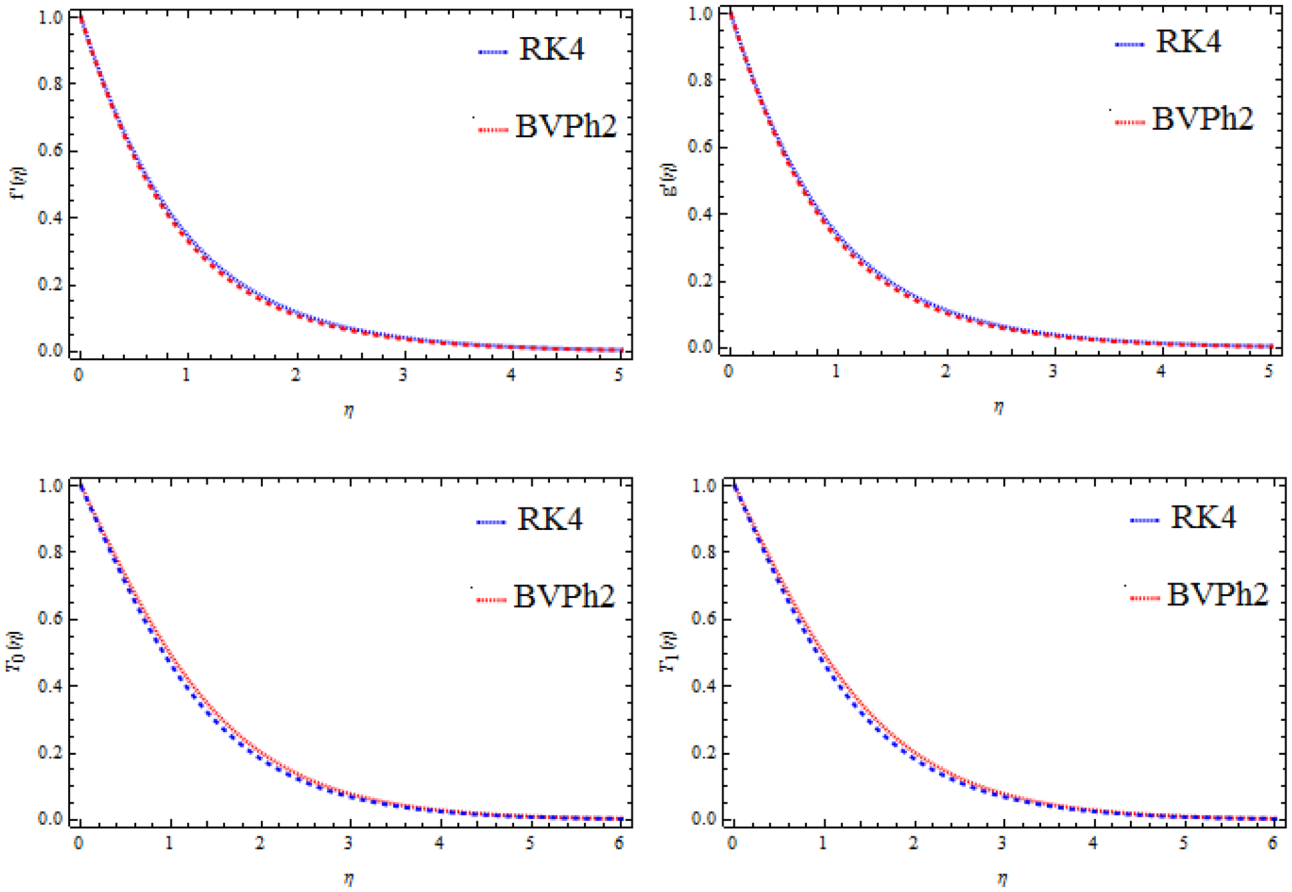

Figure 3. Comparison of RK4 and BVPh2, for velocities f' and g' and mass transfer T_0 and T_1.

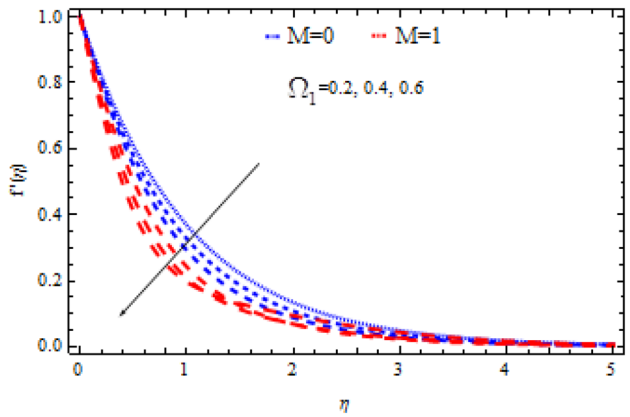

Figure 4. Consequence of Ω_1 on f'.

Table 1 shows the variation of surface mass transfer $-T_0'(0)$ and $-T_1'(0)$ for some values of Sc, Υ, M, and $\Omega_1 = \Omega_2$. From this table, it is observed that the values mass transfer $-T_0'(0)$ increases for Sc, Υ, and $\Omega_1 = \Omega_2$ whereas declines for increasing M. Similarly, the amount of $-T_1'(0)$ enhances with the increasing values of Sc, M, and $\Omega_1 = \Omega_2$ and reduces for large values of Υ. For confirmation of the present work calculation, the existing work is also compared with published work reported by Liao[21] for surface mass transfer $-T_0'(0)$ and $-T_1'(0)$, and excellent agreement is found as shown in table below.

Closing remarks

The mass transfer inside the magnetohydrodynamics free convection movement of a Jeffrey liquid limited by a stretching/shrinking surface is examined in this paper. The concentration and velocity profiles are calculated. For the numerical solutions, the Runge–Kutta fourth order method is used. For the conformation of code bvp4c

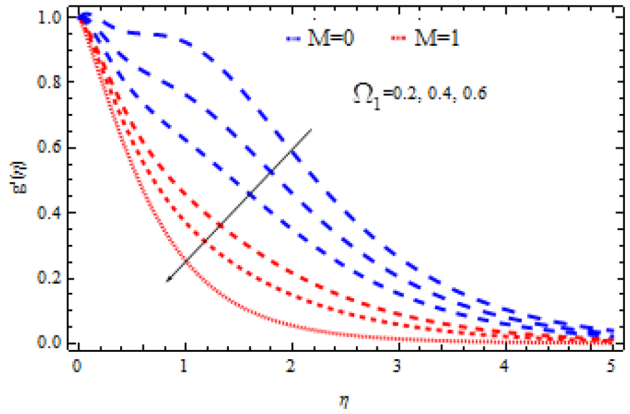

Figure 5. Consequence of Ω_1 on g'.

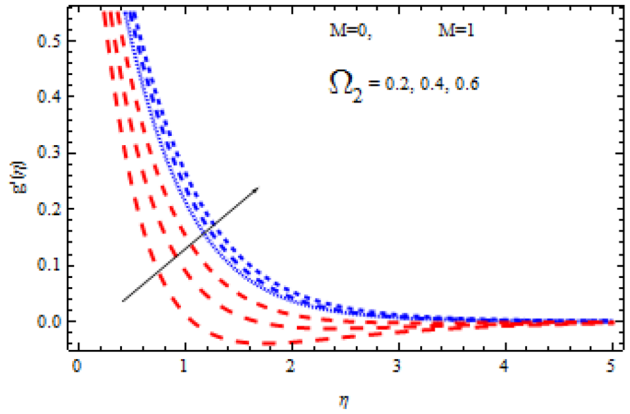

Figure 6. Consequence of Ω_2 on f'.

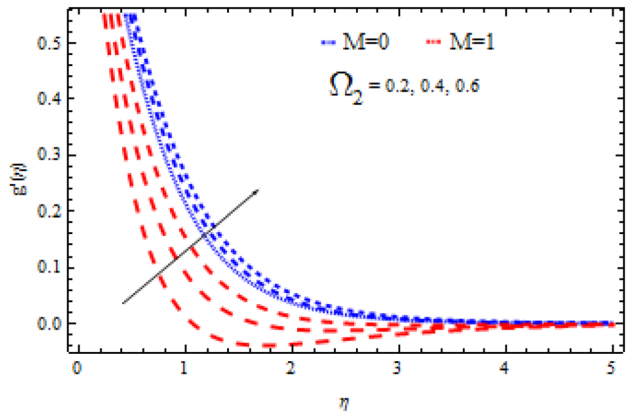

Figure 7. Consequence of Ω_2 on g'.

is also applied and excellent agreement is found The behaviour of numerous entrenched factors in the modelling under consideration is investigated. In tabular formats, the gradient of mass transfer is also estimated. The most important points are highlighted here.

1. On f' and g', the performance of Ω_1 and M_1 is same.
2. The boundary-layer thickness is reduced when the value of M_1 is increased.

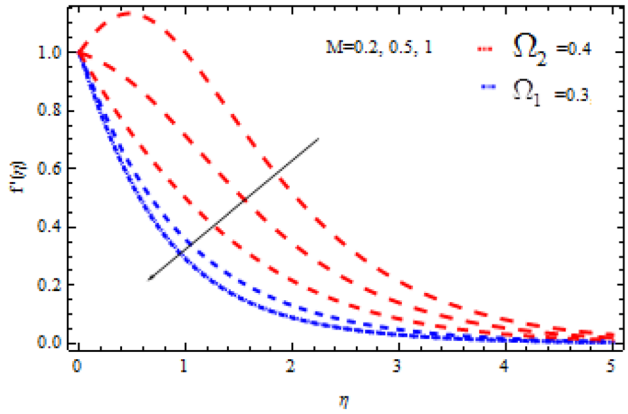

Figure 8. Consequence of M on f'.

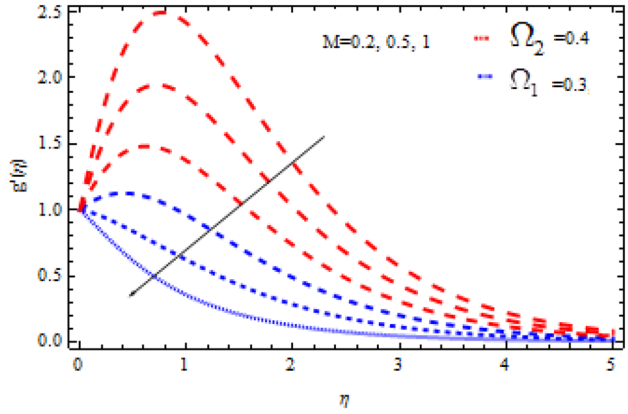

Figure 9. Consequence of M on g'.

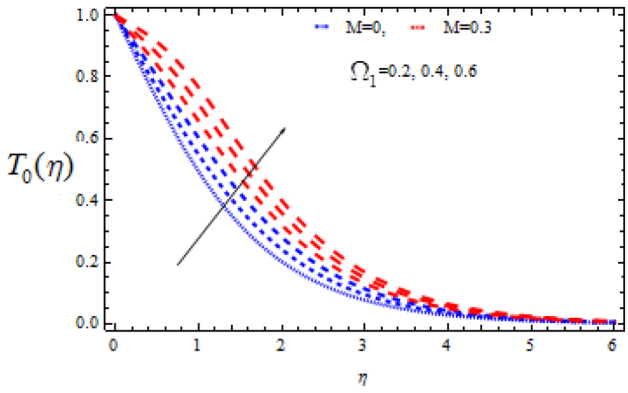

Figure 10. Consequence of Ω_1 on $T_0(\eta)$.

3. As Sc grows, the concentration fields T_0 and T_1 decline.
4. The destructive response ($\Upsilon > 0$) has the effect of lowering the concentration profiles.
5. For destructive ($\Upsilon > 0$) and generative ($\Upsilon < 0$) chemical reactions, the concentration fields T_0 and T_1 observed opposite effects.
6. By rising M, the surface mass transfer reduces.

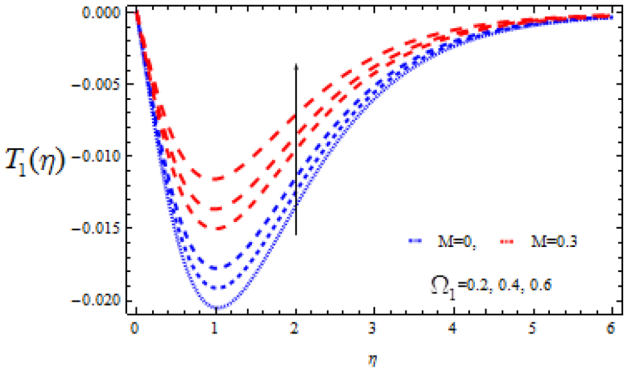

Figure 11. Consequence of Ω_1 on $T_1(\eta)$.

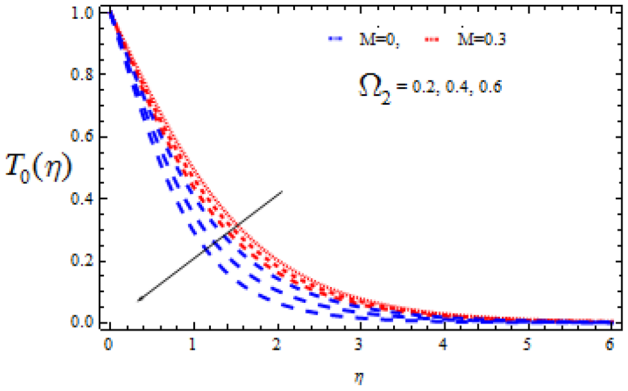

Figure 12. Consequence of Ω_2 on $T_0(\eta)$.

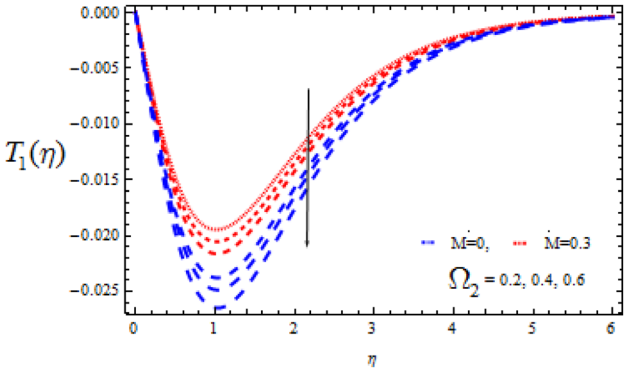

Figure 13. Consequence of Ω_2 on $T_1(\eta)$.

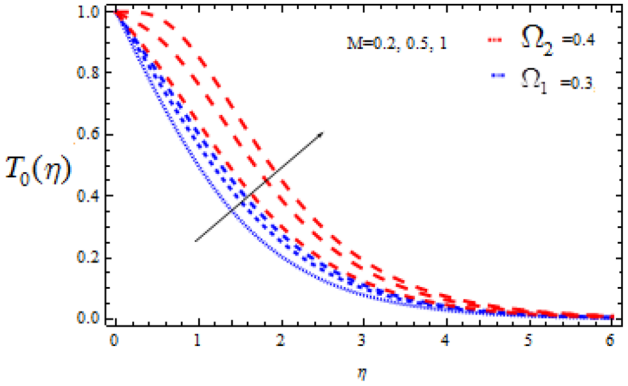

Figure 14. Consequence of M on $T_0(\eta)$.

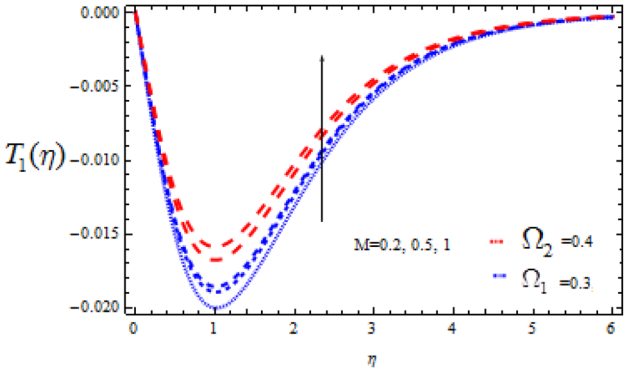

Figure 15. Consequence of M on $T_1(\eta)$.

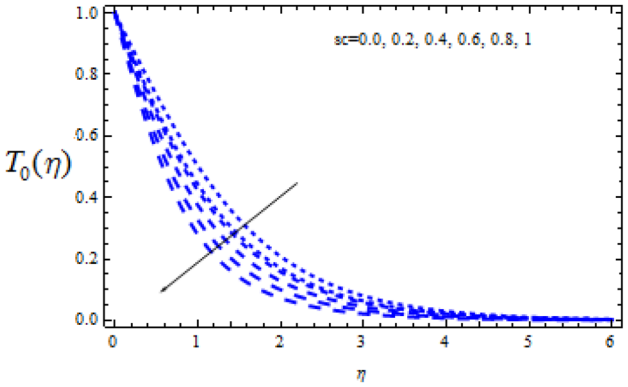

Figure 16. Consequence of Sc on $T_0(\eta)$.

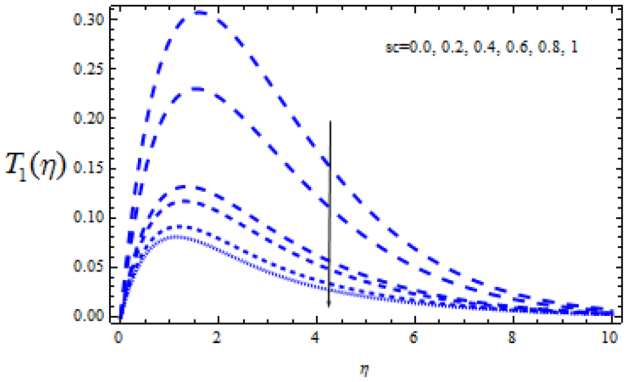

Figure 17. Consequence of Sc on $T_1(\eta)$..

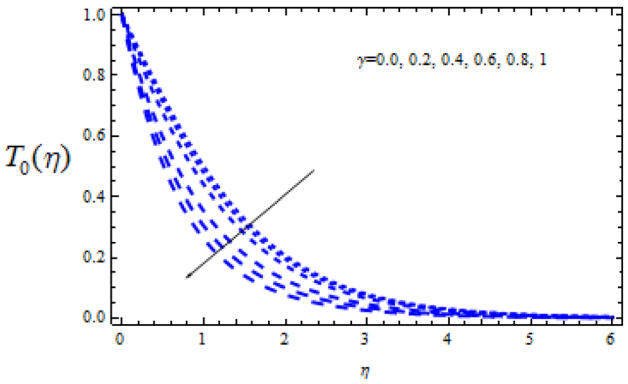

Figure 18. Consequence of Υ on $T_0(\eta)$.

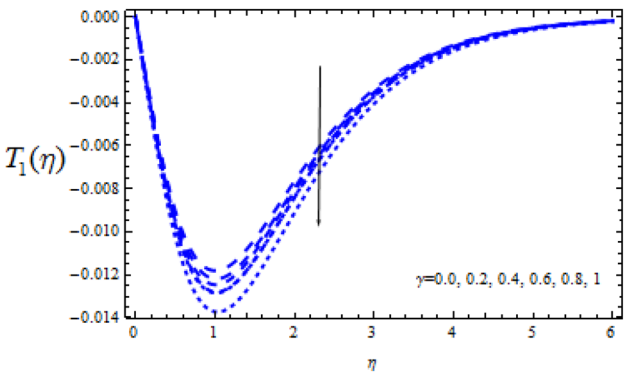

Figure 19. Consequence of Υ on $T_1(\eta)$.

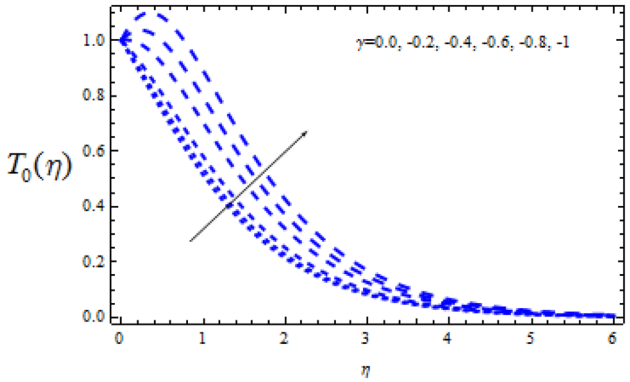

Figure 20. Consequence of Υ on $T_0(\eta)$.

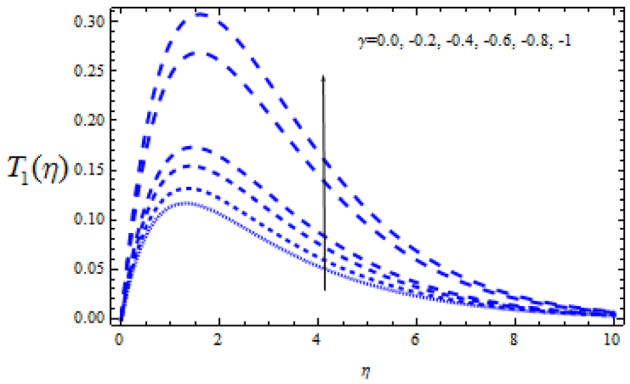

Figure 21. Consequence of Υ on $T_1(\eta)$.

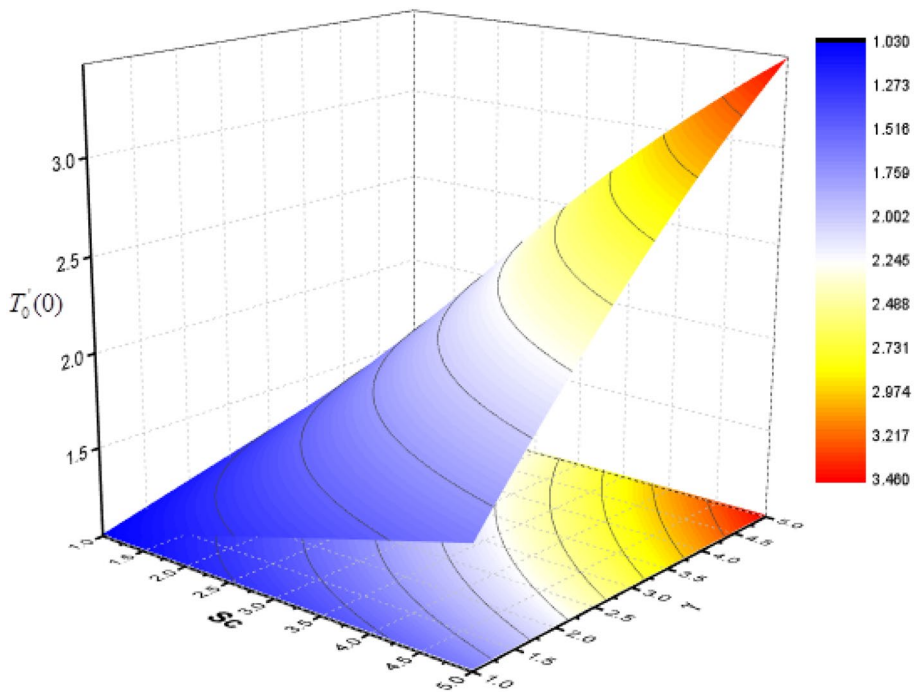

Figure 22. Consequence of Sc and Υ on $T_0'(0)$.

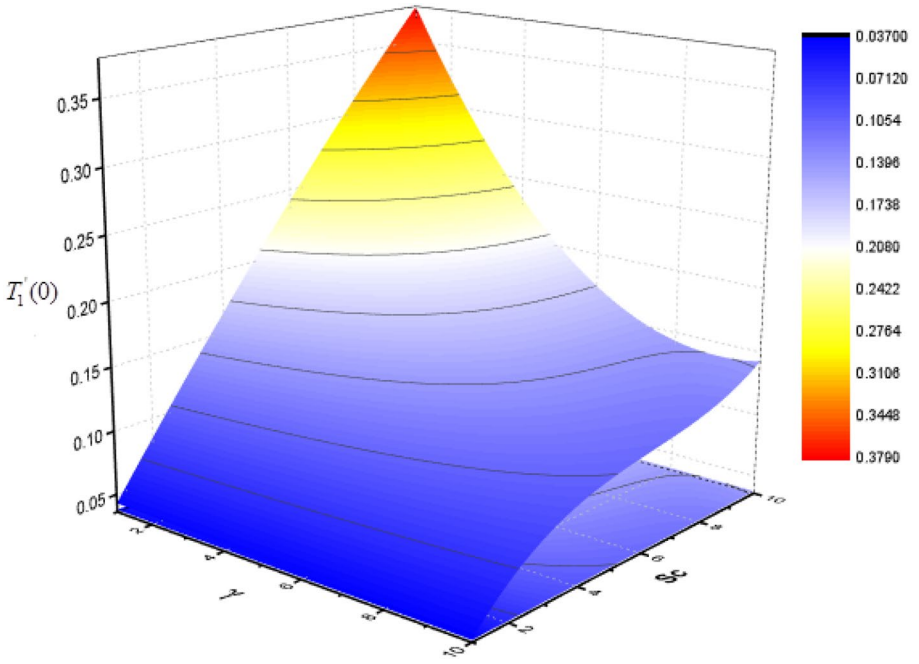

Figure 23. Consequence of Sc and Υ on $T_1'(0)$.

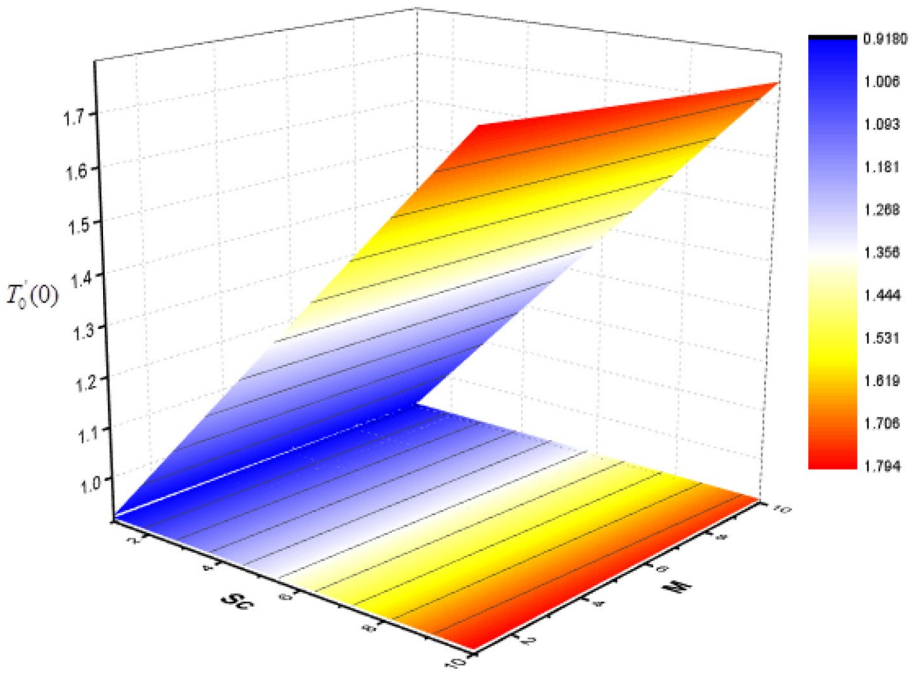

Figure 24. Consequence of Sc and M on $T_0'(0)$.

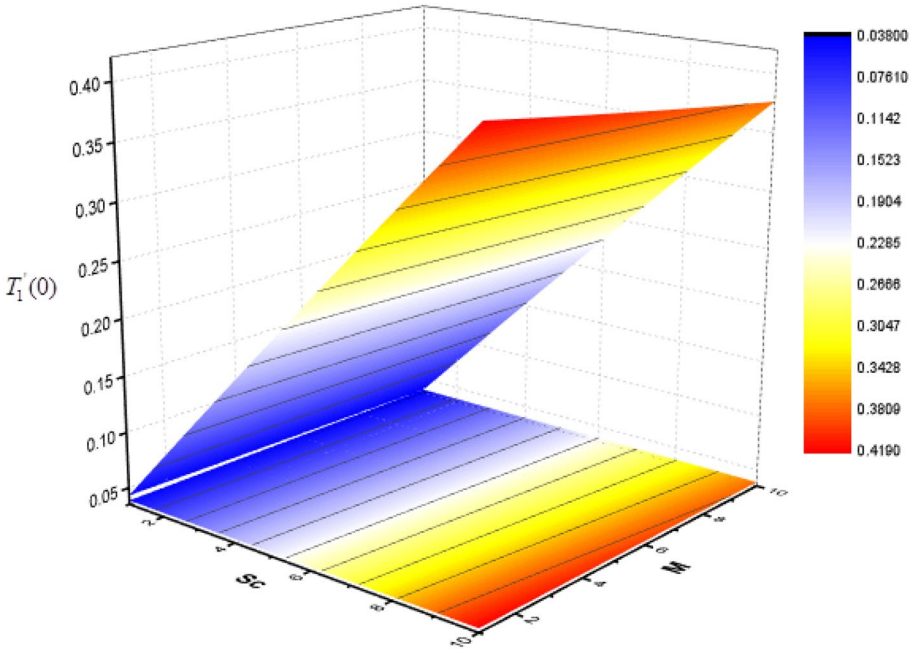

Figure 25. Consequence of *Sc* and *M* on $T_1'(0)$.

Data availability

The database used and analysed during the current study are available from the corresponding author on reasonable request.

Received: 16 January 2022; Accepted: 6 June 2022
Published online: 21 June 2022

References

1. Sakiadis, B. C. Boundary-layer behavior on continuous solid surfaces: I. Boundary-layer equations for two-dimensional and axisymmetric flow. *AIChE J.* **7**(1), 26–28 (1961).
2. Wang, C. Y. Review of similarity stretching exact solutions of the Navier–Stokes equations. *Eur. J. Mech.-B/Fluid.* **30**(5), 475–479 (2011).
3. Ishak, A., Nazar, R. & Pop, I. Hydromagnetic flow and heat transfer adjacent to a stretching vertical sheet. *Heat Mass Transf.* **44**(8), 921–927 (2008).
4. Liao, S. An analytic solution of unsteady boundary-layer flows caused by an impulsively stretching plate. *Commun. Nonlinear Sci. Numer. Simul.* **11**(3), 326–339 (2006).
5. Abbas, Z., Wang, Y., Hayat, T. & Oberlack, M. Hydromagnetic flow in a viscoelastic fluid due to the oscillatory stretching surface. *Int. J. Non-Linear Mech.* **43**(8), 783–793 (2008).
6. Liao, S. A new branch of solutions of boundary-layer flows over an impermeable stretched plate. *Int. J. Heat Mass Transf.* **48**(12), 2529–2539 (2005).
7. Hayat, T., Abbas, Z. & Ali, N. MHD flow and mass transfer of a upper-convected Maxwell fluid past a porous shrinking sheet with chemical reaction species. *Phys. Lett. A* **372**(26), 4698–4704 (2008).
8. Hayat, T., Sajid, M. & Pop, I. Three-dimensional flow over a stretching surface in a viscoelastic fluid. *Nonlinear Anal. Real World Appl.* **9**(4), 1811–1822 (2008).
9. Alizadeh-Pahlavan, A. & Sadeghy, K. On the use of homotopy analysis method for solving unsteady MHD flow of Maxwellian fluids above impulsively stretching sheets. *Commun. Nonlinear Sci. Numer. Simul.* **14**, 1355 (2009).
10. Ariel, P. D., Hayat, T. & Asghar, S. The flow of an elastico-viscous fluid past a stretching sheet with partial slip. *Acta Mech.* **187**(1), 29–35 (2006).
11. Vajravelu, K. Viscous flow over a nonlinearly stretching sheet. *Appl. Math. Comput.* **124**(3), 281–288 (2001).
12. Vajravelu, K. & Cannon, J. R. Fluid flow over a nonlinearly stretching sheet. *Appl. Math. Comput.* **181**(1), 609–618 (2006).
13. Cortell, R. Effects of viscous dissipation and radiation on the thermal boundary layer over a nonlinearly stretching sheet. *Phys. Lett. A* **372**(5), 631–636 (2008).
14. Cortell, R. Viscous flow and heat transfer over a nonlinearly stretching sheet. *Appl. Math. Comput.* **184**(2), 864–873 (2007).
15. Hayat, T., Abbas, Z. & Javed, T. Mixed convection flow of a micropolar fluid over a non-linearly stretching sheet. *Phys. Lett. A* **372**(5), 637–647 (2008).
16. Raptis, A. & Perdikis, C. Viscous flow over a non-linearly stretching sheet in the presence of a chemical reaction and magnetic field. *Int. J. Non-Linear Mech.* **41**(4), 527–529 (2006).
17. Liao, S. *Beyond Perturbation: Introduction to the Homotopy Analysis Method* (Chapman and Hall/CRC, 2003).
18. Liao, S. Notes on the homotopy analysis method: some definitions and theorems. *Commun. Nonlinear Sci. Numer. Simul.* **14**(4), 983–997 (2009).
19. Hashim, I., Abdulaziz, O. & Momani, S. Homotopy analysis method for fractional IVPs. *Commun. Nonlinear Sci. Numer. Simul.* **14**(3), 674–684 (2009).
20. Abbasbandy, S. Solitary wave solutions to the modified form of Camassa-Holm equation by means of the homotopy analysis method. *Chaos, Solitons Fractals* **39**(1), 428–435 (2009).

21. Liao, S. J. A general approach to get series solution of non-similarity boundary-layer flows. *Commun. Nonlinear Sci. Numer. Simul.* **14**(5), 2144–2159 (2009).
22. Abbasbandy, S. Approximate solution for the nonlinear model of diffusion and reaction in porous catalysts by means of the homotopy analysis method. *Chem. Eng. J.* **136**(2–3), 144–150 (2008).
23. Hayat, T., Javed, T. & Abbas, Z. MHD flow of a micropolar fluid near a stagnation-point towards a non-linear stretching surface. *Nonlinear Anal. Real World Appl.* **10**(3), 1514–1526 (2009).
24. Hayat, T. & Abbas, Z. Heat transfer analysis on the MHD flow of a second grade fluid in a channel with porous medium. *Chaos, Solitons Fractals* **38**(2), 556–567 (2008).
25. Abbas, Z. & Hayat, T. Radiation effects on MHD flow in a porous space. *Int. J. Heat Mass Transf.* **51**(5–6), 1024–1033 (2008).
26. Hayat, T., Abbas, Z. & Pop, I. Mixed convection in the stagnation point flow adjacent to a vertical surface in a viscoelastic fluid. *Int. J. Heat Mass Transf.* **51**(11–12), 3200–3206 (2008).
27. Abbasbandy, S., Babolian, E. & Ashtiani, M. Numerical solution of the generalized Zakharov equation by homotopy analysis method. *Commun. Nonlinear Sci. Numer. Simul.* **14**(12), 4114–4121 (2009).
28. Abbasbandy, S. & Parkes, E. J. Solitary smooth hump solutions of the Camassa-Holm equation by means of the homotopy analysis method. *Chaos, Solitons Fractals* **36**(3), 581–591 (2008).
29. Liao, S. An optimal homotopy-analysis approach for strongly nonlinear differential equations. *Commun. Nonlinear Sci. Numer. Simul.* **15**(8), 2003–2016 (2010).
30. Niu, Z. & Wang, C. A one-step optimal homotopy analysis method for nonlinear differential equations. *Commun. Nonlinear Sci. Numer. Simul.* **15**(8), 2026–2036 (2010).
31. Akoh, H., Tsukasaki, Y., Yatsuya, S. & Tasaki, A. Magnetic properties of ferromagnetic ultrafine particles prepared by vacuum evaporation on running oil substrate. *J. Cryst. Growth* **45**, 495–500 (1978).
32. Kuznetsov, A. V. The onset of nanofluid bioconvection in a suspension containing both nanoparticles and gyrotactic microorganisms. *Int. Commun. Heat Mass Transfer* **37**(10), 1421–1425 (2010).
33. Varun Kumar, R. S., PunithGowda, R. J., Naveen Kumar, R., Radhika, M. & Prasannakumara, B. C. Two-phase flow of dusty fluid with suspended hybrid nanoparticles over a stretching cylinder with modified Fourier heat flux. *SN Appl. Sci.* **3**(3), 1–9 (2021).
34. Manjunatha, P. T. *et al.* Significance of stefan blowing and convective heat transfer in nanofluid flow over a curved stretching sheet with chemical reaction. *J. Nanofluids* **10**(2), 285–291 (2021).
35. Madhukesh, J. K., Alhadhrami, A., Naveen Kumar, R., Punith Gowda, R. J., Prasannakumara, B. C. & Varun Kumar, R. S. Physical insights into the heat and mass transfer in Casson hybrid nanofluid flow induced by a Riga plate with thermophoretic particle deposition. *Proc. Inst. Mech. Eng., Part E: J. Process Mech. Eng.*, 09544089211039305.
36. Saad, H. & Asker, H. G. An unconditionally stable finite-difference method for the solution of multi-dimensional transport equation. *Ain Shams Engi. J.* **12**(1), 807–820 (2021).
37. Barakat, H. Z., Kamal, M. M., Saad, H. E. & Ibrahim, B. Blending effect between the natural gas and the liquefied petroleum gas using multiple co-and cross-flow jets on NOx emissions. *Ain Shams Eng. J.* **10**(2), 419–434 (2019).
38. Turkyilmazoglu, M. Thermal management of parabolic pin fin subjected to a uniform oncoming airflow: Optimum fin dimensions. *J. Therm. Anal. Calorim.* **143**(5), 3731–3739 (2021).
39. Turkyilmazoglu, M. Heat and mass transfer on the MHD fluid flow due to a porous rotating disk with hall current and variable properties (2011).
40. Turkyilmazoglu, M. MHD natural convection in saturated porous media with heat generation/absorption and thermal radiation: Closed-form solutions. Arch. Mech. **71**(1) (2019).
41. Turkyilmazoglu, M. Suspension of dust particles over a stretchable rotating disk and two-phase heat transfer. *Int. J. Multiph. Flow* **127**, 103260 (2020).
42 Türkyilmazoğlu, M. Nonlinear problems via a convergence accelerated decomposition method of Adomian. *Compu. Model. Eng. Sci.* **127**(1), 1–22 (2021).
43. Turkyilmazoglu, M. Retraction notice to MHD Fluid Flow and Heat Transfer with Varying Prandtl Numbers Due to a Rotating Disk Subject to a Uniform Radial Electric Field ATE, 127–133 (2018)

Author contributions

Z.: Conceptualization, Data curation, Writing—original draft, Methodology, Investigation. I.K. and N.F.: Conceptualization, Resources, Visualization. F.S. Al-D.: Revised the manuscript, corrected the model and provide results that are grid-independent. O.M.: Explained the novelty. F.S. Al-D. and O.M.: Developed the code (Wolfram Mathematica 7.0.18.43403, Version 12.0.0, Developed by Wolfram Research, Inc.), Made correction with author's response. F.S. Al-D. and O.M.: Validate Writing—review and editing.

Competing interests

The authors declare no competing interests.

Additional information

Correspondence and requests for materials should be addressed to Z.

Reprints and permissions information is available at www.nature.com/reprints.

Publisher's note Springer Nature remains neutral with regard to jurisdictional claims in published maps and institutional affiliations.